Luminescent Lanthanide-Functionalized Gold Nanoparticles: Exploiting the Interaction with Bovine Serum Albumin for Potential Sensing Applications

Steve Comby* **and Thorfinnur Gunnlaugsson***

School of Chemistry, Centre for Synthesis and Chemical Biology, Trinity College Dublin, Dublin 2, Ireland

ABSTRACT As luminescent surface-functionalized gold nanoparticles emerged as potential powerful analytical tools in the biomedical fields, understanding the interaction of such systems with proteins has become crucial. In the present study, the interaction of luminescent water-soluble gold nanoparticles (AuNP-1·Eu-nta), obtained through the self-assembly of a naphthalene β-diketone antenna with a Eu(III) cyclen complex tethered to the gold surface *via* a C_{12} alkyl thiol spacer, with bovine serum albumin (BSA) was investigated. The changes in the UV–visible absorption and fluorescence spectra of both the antenna and protein, as well as in the time-resolved Eu(III)-centered emission, of the resulting self-assembly were monitored, at physiological pH, as a function of the BSA concentration. We demonstrate that the Eu(III) emission arising from the self-assembly on the AuNP surface is almost completely quenched upon addition of BSA. Binding constant determination clearly showed that the sensitizing antenna was not displaced and that the quenching was the result of the interaction between the antenna and BSA. Detailed spectroscopic studies performed on the nta–BSA system brought a better insight in the strength of such interaction as well as its effect on the protein secondary structure. Finally, the information gathered on each system resulted in applying AuNP-1·Eu-nta–BSA for the luminescent detection of drugs *via* the perturbation of the nta–BSA interaction. Competitive titrations using ibuprofen and warfarin showed that nta was located in the binding site II of BSA and that the presence of warfarin, a site I drug, did not interfere with the detection of site II ibuprofen.

KEYWORDS: Eu(III)-functionalized gold nanoparticles · luminescent ternary complex · bovine serum albumin · protein–nanoparticle interaction · luminescence quenching · competitive displacement assay

The design and development of novel functional hybrid nanomaterials is of great current interest in supramolecular chemistry and nanochemistry, particularly for applications in biotechnology, such as sensing, molecular diagnostics, and imaging. Systems such as quantum dots and metal nanoparticles (NPs), which exhibit interesting and tunable, size- and shape-dependent properties, have been widely developed during the past decade,[1–3] where they have found applications in drug delivery,[3–5] cancer research,[6,7] such as photodynamic therapy,[8] and tissue engineering.[5,9] In particular, gold nanoparticles (AuNPs) have attracted much attention owing to their biocompatibility and their relatively simple functionalization with various organic and biological molecules.[10–12] To date, the detection and sensing of various analytes using AuNP systems is well established and is commonly based on observing the changes in the surface plasmon resonance (SPR) absorption band of the AuNPs themselves, upon recognition or binding of the analytes.[13–15] In contrast, the use of fluorophore-functionalized AuNPs has been less explored for sensing,[16] the reason being that AuNPs and other metal-based nanoparticles have often proved to be efficient luminescence quenchers.[17,18] Therefore, the use of fluorescence spectroscopy, even though being more sensitive than UV–visible absorption spectroscopy, is usually avoided for studying the sensing ability of such AuNPs-based systems. Nevertheless, recent studies have shown that such quenching can be circumvented[16,19,20] and also demonstrated that, in most of the cases, the quenching efficiency of AuNPs is strongly distance dependent and, thus, can be minimized by increasing the separation (longer spacer) between the gold surface and the fluorophores.[21,22]

Concomitantly, lanthanide (Ln) complexes have been widely used as luminescent tools for optical imaging and sensing of biological species due to their unique photophysical properties, such as long-lived excited states (μs–ms range) and narrow, easily recognizable line-like emission bands (with large Stokes' shifts) in either the visible or near-infrared region.[23–30] These characteristics are highly attractive for biological use compared to commonly used fluorophores, as they allow overcoming autofluorescence and light scattering from the biological samples and, hence, provide a significant signal-to-noise ratio enhancement.[26]

* Address correspondence to combys7@gmail.com; gunnlaut@tcd.ie.

Received for review May 30, 2011 and accepted August 25, 2011.

Published online August 26, 2011
10.1021/nn201992z

The potential of such Ln-based probes for the luminescent sensing of biological substrates can be further enhanced by conjugating lanthanide complexes to NPs. Indeed, such functionalization allows high loading of probes/sensors/imaging agents, *etc.*, while possibly improving both the selectivity and sensitivity of such a device.[31,32] Furthermore, the presence of large numbers of complexes on the NP surface can also allow for the detection of several analytes in a single assay; moreover, the targeting of larger biological structures through multiple binding site interactions is also possible with such structures.[1] Most of the luminescent Ln-based NPs developed to date are based on silica,[31−34] polystyrene,[35,36] or quantum dot[37] NPs, and only a few examples of luminescent Ln-functionalized AuNPs have been reported.[38−41] Recently, we showed that the heptadentate Eu(III) macrocyclic cyclen complex 2·Eu, used previously in our group to form luminescent ternary complexes with carboxylates and β-diketonates[23,42] in aqueous solution, can be synthetically modified[43] to allow for the introduction of an alkyl thiol group at the free amino moiety of 2·Eu, yielding 1·Eu, which enabled the adsorption of this complex onto the surface of AuNPs. Addition of a well-suited antenna to the water-soluble Eu(III)-functionalized AuNPs resulted in the formation of highly red-emitting ternary complexes on the surface of the AuNPs upon excitation of the antenna, the characteristic Eu(III) emission being sensitized *via* energy transfer from the antenna triplet state.[23,26,27,42] This particular system was shown to behave in a similar manner when attached to a flat gold surface.[44] We further demonstrated the application of this design for use in displacement assays, with the sensing of biologically relevant anions in aqueous solution.[40]

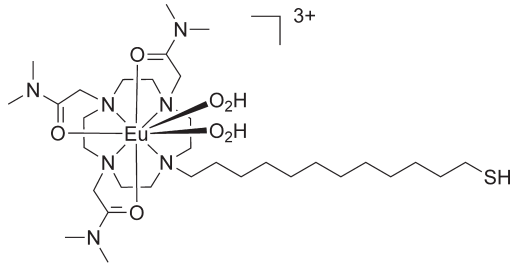

1·Eu

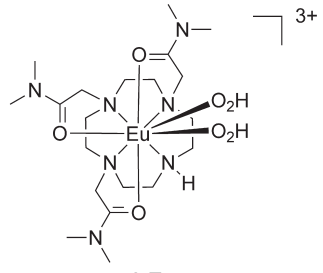

2·Eu

With the interest for these new types of functional nanomaterials growing considerably, great attention has to be put on how such nanoprobes, having comparable sizes to biomolecules, interact with the biological system and more particularly with proteins.[45−47] Indeed, it has been shown that NPs could bind/absorb many plasma proteins, with either negative or positive outcomes; for instance, the protein coating can enhance the stability of NPs or assist cell internalization, where the surface charges dramatically affect the cellular uptake of AuNPs.[48,49] On the other hand, interactions with NPs have been found to induce protein aggregation, misfolding, and deactivation (loss of protein activity) and could also affect protein−protein interactions, possibly resulting in protein malfunctioning, which ideally should be avoided.[50,51] In the present study, we evaluated the interaction of the luminescent AuNP-1·Eu-nta system with proteins, focusing our current study on the use of serum albumin, which has previously been shown to bind to lanthanide complexes,[52,53] such as cyclen-based systems,[54−58] while concomitantly being the main plasma carrier for a wealth of both endogenous and exogenous substances.[59] The influence on the luminescent properties of both AuNP-1·Eu-nta and bovine serum albumin (BSA) has been carefully examined, and the data obtained were fitted using linear and nonlinear regression analysis to determine the binding constants for the different species formed in solution. Taking advantage of the relatively strong interaction occurring between these two components, this system was further exploited as a site II selective drug sensor at physiological pH and its applicability demonstrated using the two universal drugs warfarin and ibuprofen.

RESULTS AND DISCUSSION

Eu(III) Cyclen-Capped Gold Nanoparticles. We reported previously the synthesis of 1·Eu and its use to functionalize the surface of AuNPs, yielding the water-soluble system AuNP-1·Eu; see schematic representation in Scheme 1.[40]

The functionalized AuNP-1·Eu synthesized in the present work was stable in buffered solution, and no aggregation was observed through time, as confirmed by the characteristic gold SPR absorption band at ~515 nm. Similarly, transmission electron microscopy (TEM) images indicated the presence of monodispersed spherical nanoparticles, Figure 1A, with an average gold core diameter of ~5 nm (TEMs of all batches gave rise to similar images as shown in Figure 1A). These results were further corroborated by measuring the actual functionalized AuNP spherical size, including the 1·Eu capping layer, and their distribution in solution using dynamic light scattering (DLS), Figure 1B. The measurements showed that the average hydrodynamic diameter of AuNP-1·Eu in water was 12.8 nm, with the nanoparticle distribution (5.6−28.2 nm range) reaching a maximum at 11.7 nm. On the basis of MM2 calculations performed on the 1·Eu complex, the maximum distance between the

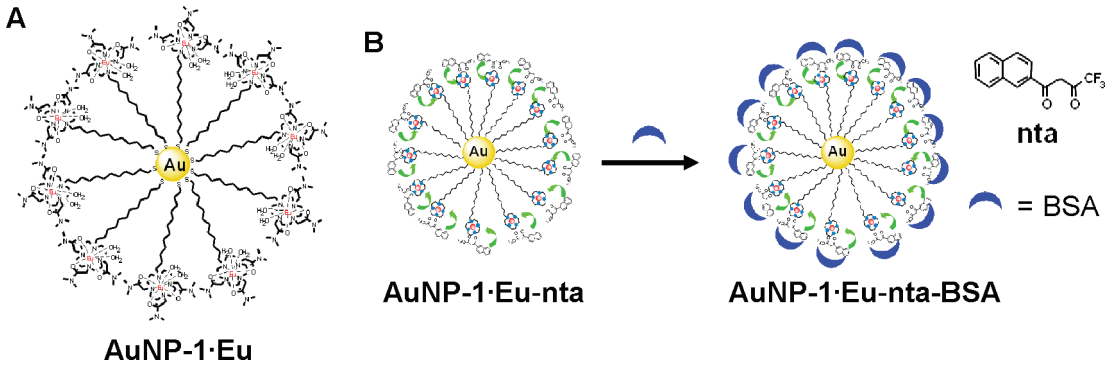

Scheme 1. Schematic representation of AuNP-1·Eu, AuNP-1·Eu-nta, and AuNP-1·Eu-nta−BSA. (A) Cyclen complex 1·Eu conjugated to AuNP, giving AuNP-1·Eu (each NP has *ca.* 120 1·Eu complexes; see Figure 2). (B) The binding of nta gives the luminescent ternary complexes AuNP-1·Eu-nta, which then interact with BSA to give AuNP-1·Eu-nta−BSA. BSA is shown here schematically as interacting with AuNP-1·Eu-nta; the exact number of BSA is not known, although the number of equivalents needed to quench the Eu(III) emission is in agreement with the number of BSA found to be associated with AuNP; see discussion below.

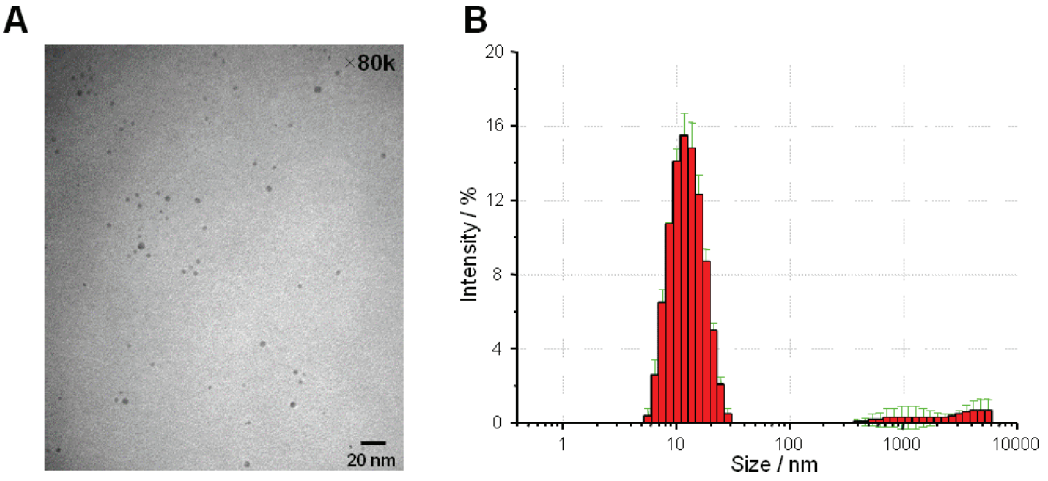

Figure 1. Size characterization of the functionalized gold nanoparticles, AuNP-1·Eu: (A) TEM image (a representation of the many TEM images recorded as part of this work) of the gold core and (B) DLS analysis of the same AuNP in water.

thiol group binding to the gold surface and the most external dimethyl acetamide arm was calculated to be around 23.6 Å. If this distance is added twice to the average gold nanoparticle core diameter obtained by TEM analysis, the estimated diameter is matching the experimental values determined by DLS (Figure S1, Supporting Information), considering that the light scattering from the gold core and that of the capping layer are different, and the effect of both are not just additive.

Due to the absence of a sensitizing antenna in 1·Eu, combined with the presence of two metal-bound water molecules, the Eu(III)-centered emission was found to be weak upon direct excitation of the metal ion. We have shown that the use of an external antenna such as 4,4,4-trifluoro-1-(2-naphthyl)-1,3-butanedione (Hnta) allows the displacement of the aforementioned two metal water molecules,[42] while concomitantly offering an efficient sensitization of the metal center. This was clearly visible by the appearance of the characteristic Eu(III) emission in the 570−720 nm range upon titrating 1·Eu with nta in HEPES-buffered solution. The changes in the Eu(III) $^5D_0 \rightarrow {}^7F_J$ (J = 0−4) transitions upon antenna excitation at 330 nm revealed the formation of a 1:1 ternary complex, 1·Eu-nta, involving the direct coordination of the antenna to the lanthanide ion. The formation of such luminescent ternary complexes has been used to estimate the number of 1·Eu complexes attached onto the AuNP surface. In the present work, titrations of AuNP-1·Eu (0.1 μM) with nta showed that *ca.* 120 ± 20 complexes were covalently linked to each AuNP (Figure 2). Sensitization of the Eu(III) emission by nta is ascertained by the excitation spectrum monitored at 617 nm, which closely matches the absorption spectrum of the diketone, as shown in Figure S2A, Supporting Information. It is important to notice that upon excitation of AuNP-1·Eu-nta at 330 nm, both ligand- and metal-centered luminescence are observed; the residual nta fluorescence indicates that even if the sensitization of the Eu(III) emission is efficient, the energy transfer to the metal center is not complete.

Interaction of AuNP-1·Eu-nta with BSA. The photophysical properties of AuNP-1·Eu-nta at physiological pH, in the presence of BSA, were investigated by using UV−visible spectroscopy as well as both steady-state and time-resolved luminescence techniques. Luminescent NPs were prepared prior to each BSA titration by adding 120 equivalents of nta to a solution of AuNP-1·Eu (0.1 μM) in Hepes buffer. Addition of BSA to the solution resulted in a significant quenching of the Eu(III) emission from AuNP-1·Eu-nta, where at high protein loading (675 equivalents) more than 95% of the initial luminescence was quenched, Figure 3. Analysis of the changes in the emission as a function of added BSA is shown as an inset in Figure 3A, which demonstrates that most of the quenching is observed after the addition of *ca.* 150 equivalents of BSA.

This is close to the number of estimated lanthanide complexes on AuNP-1·Eu, Figure 2, as well as being in good agreement with the work of Feldheim *et al.*,[60] who have shown that *ca.* 160 $[Ru(2,2'\text{-bipyridine})_3]^{2+}$-labeled BSA complexes were found to be associated on each 20 nm diameter AuNP, using time-correlated single-photon counting measurements. Similar quenching behavior in the presence of serum albumin was recently observed to a lesser extent for both Eu(III) and Tb(III) cyclen-based complexes, incorporating an azaxanthone sensitizing unit, where Parker and coworkers[55] attributed the partial loss of the Ln-centered emission to be consistent with static quenching of the azaxanthone excited state by the HSA protein.

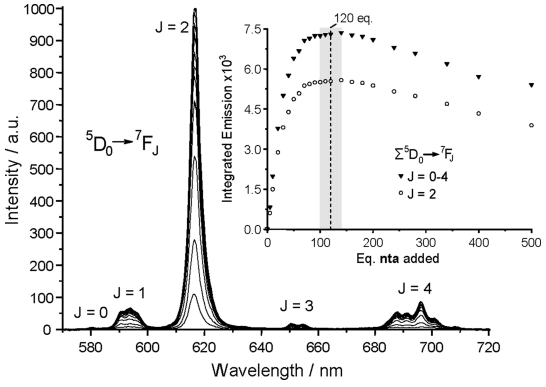

Figure 2. Changes in the Eu-centered emission of AuNP-1·Eu (10^{-7} M) in Hepes-buffered solution (pH 7.4) upon addition of nta (0−500 equivalents) at 298 K; λ_{ex} = 330 nm. Inset: Changes in the Eu(III) emission integrals for J = 0−4 and J = 2 *vs* the number of equivalents of nta added.

The "switching off" of the Eu(III) emission in the presence of BSA was investigated to determine the origin of the quenching. For this purpose, both the excitation spectra and the Eu($^5D_0$) excited-state lifetimes were measured. The excitation spectra displayed the same feature throughout the titration, with an intense band centered at 343 nm and with a further two less intense bands in the 250−300 nm range. Normalization of the spectra demonstrated that the contribution from the higher energy excitation bands (relative to the lower energy one) continuously weakened upon addition of BSA (see Figure S2B). This behavior is explained by the strong absorption of BSA in the 250−300 nm range, which implies that the protein fluorophores (tryptophan and tyrosine moieties) do not participate, or only to a small extent if they do, in the sensitization of the Eu(III) emission in the presence of nta.

The luminescence decays, obtained upon excitation through the nta electronic levels at 330 nm, were best fitted to a double-exponential function, in both the absence and presence of BSA (see Figure S3). The corresponding lifetimes of the $^5D_0$ excited state of Eu(III) as a function of the equivalents of BSA added, their relative contribution to the total luminescence decay, and the average lifetime values (see Experimental Section) are summarized in Table S1. In the

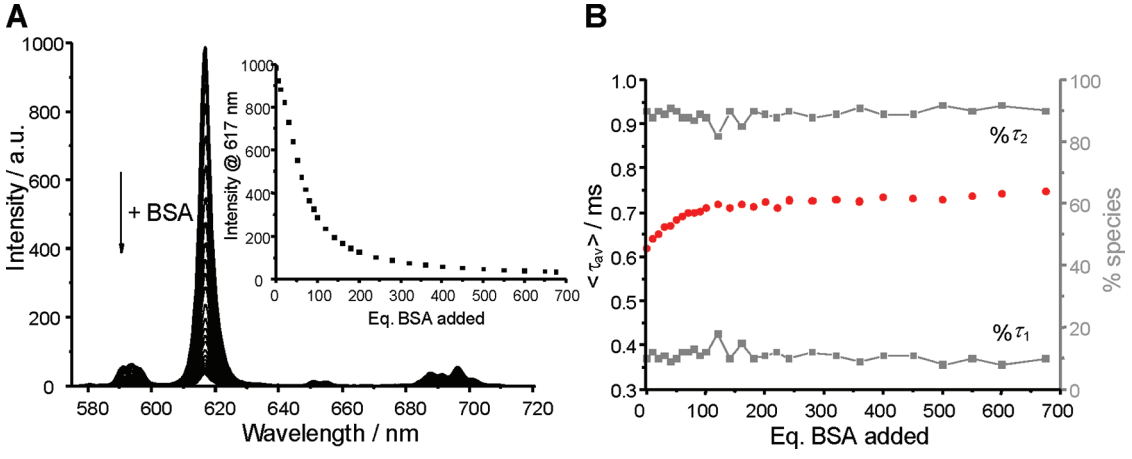

Figure 3. (A) Evolution of the Eu(III) emission of AuNP-1·Eu-nta upon titration with BSA in Hepes buffer (pH 7.4). Inset: Intensity changes observed for the Eu(III) $^5D_0 \rightarrow {}^7F_2$ transition *vs* equivalents of BSA added; [AuNP-1·Eu] = 10^{-7} M, [nta] = 1.2 × 10^{-5} M, and λ_{ex} = 330 nm. (B) Average lifetimes of the Eu($^5D_0$) excited state as a function of the equivalents of BSA added to a solution of AuNP-1·Eu-nta. The gray scale displays the percentages of each species calculated from the lifetimes obtained (see Table S1).

absence of BSA, the AuNP-1·Eu-nta system was characterized by two lifetimes, measured as $\tau_1 = 0.16(2)$ ms and $\tau_2 = 0.67(2)$ ms, accounting for 10% and 90% of the total luminescence, respectively. As BSA was added, an increase in the average lifetime, $\langle\tau_{av}\rangle$, was observed before reaching a plateau around 150 equivalents, at which the maximum 20% increase was observed (Figure 3B). In contrast, only minor changes were noticed in the overall lifetime speciation, *i.e.*, in the % ratio of τ_1 and τ_2, where the longer lifetime consisted of ~90% of the total emission decay, the remaining 10% corresponding to the shorter-lived species. Therefore, the increase observed in the lifetime is likely to be caused by a shielding of the Eu(III) ion from the bulk solvent. Indeed, the addition of the relatively hydrophobic protein potentially led to a decrease in second sphere nonradiative deactivations.

To investigate further the origin of the luminescence quenching, a Hepes-buffered solution of AuNP-1·Eu was titrated with BSA (0–400 equivalents), prior to the addition of the nta antenna. It was observed that the weak metal-centered emission arising from the AuNP-1·Eu was enhanced upon addition of BSA (see Figure S4). Thus, after the addition of *ca.* 150 equivalents of BSA, a plateau was reached and the integration of the Eu(III) emission, corrected for the absorbance changes at the excitation wavelength, corresponded to ~2-fold enhancement of that observed for the Eu(III) emission in the absence of the protein. The luminescence enhancement observed was attributed to a more efficient protection of the Eu(III) ion from its environment and/or weak sensitization of the Ln-centered emission through the protein chromophoric groups, *i.e.*, tryptophan and tyrosine residues. Indeed, in the absence of any other chromophores, the latter possibility could not be ruled out. The final solution, namely, AuNP-1·Eu + 400 equivalents of BSA, was then titrated with nta, the results of which are shown in Figure 4. A significant 5-fold increase in the emission was observed after the addition of only 10 equivalents of nta, while the addition of a further 10 equivalents led to an order of magnitude enhancement (see Figure S5A).

This behavior, at such low nta:BSA ratios (*i.e.*, 1:40, 1:20), demonstrated that if an interaction occurred between the protein and the Eu-functionalized AuNP, this interaction was probably much weaker than the one between nta and the metal center itself; which is not surprising, given the fact that the β-diketonates are known to have high affinity for Ln(III) ions.[61] This theory was further verified by looking at the changes observed in the Eu(III) emission, especially in the intensity of the hypersensitive $^5D_0 \rightarrow {}^7F_2$ transition relative to the magnetic dipole one ($^5D_0 \rightarrow {}^7F_1$). Indeed, these values, shown in Table S2, clearly indicated a significant change in the Eu(III) environment upon addition of nta, even in the presence of BSA in the solution, the protein itself having only little effect on the $^7F_2/{}^7F_1$ ratio (see Figure S5B).

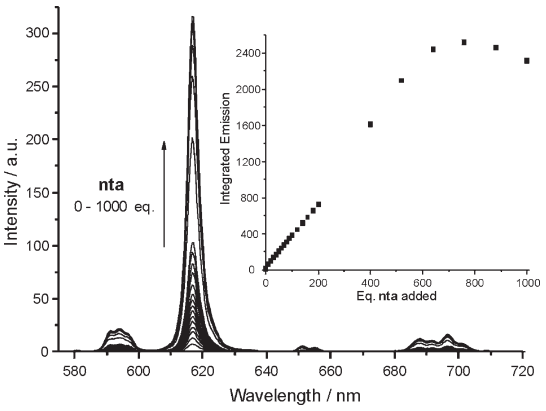

Figure 4. Evolution of the Eu(III) emission of AuNP-1·Eu-BSA upon addition of nta (0–1000 equivalents) in Hepes-buffered solution (pH 7.4); [AuNP-1·Eu] = 10^{-7} M, [BSA] = 3.78×10^{-5} M, and $\lambda_{ex} = 330$ nm. Inset: Changes observed in the emission integrals of the Eu(III) $^5D_0 \rightarrow {}^7F_J$ transitions (J = 0–4) *vs* equivalents of nta added.

Steady-state and time-resolved fluorescence measurements were also carried out on the protein itself in the absence and the presence of 1·Eu and AuNP-1·Eu, to determine the nature and strength of the interaction taking place between the lanthanide ion and the protein. The intrinsic fluorescence of BSA is mainly due to tryptophan residues, Trp-134 and Trp-212, and to a much lesser extent to tyrosine and phenylalanine residues.[59,62] Of these, Trp-134 is located at the surface of the protein, in domain I, while Trp-212 is located in domain II, buried inside the protein structure, within a hydrophobic binding pocket. The fluorescence spectrum of BSA presents a strong emission maximum at 348 nm, when excited at 278 nm in Hepes buffer solution. Conversely, the nta antenna was almost nonfluorescent under these experimental conditions, while the Eu(III) emission occurred at much lower energy. The addition of 1·Eu to BSA in Hepes buffer resulted in a significant quenching of the protein fluorescence (see Figure S6A). This quenching can be initiated by different mechanisms, usually classified as dynamic and static quenching, which can be distinguished by their differing dependence on temperature and viscosity, or preferably by lifetime measurements,[63] and hence, the influence of 1·Eu on the fluorescence lifetime of BSA was measured. The fluorescence decay of BSA in the absence and presence of 1·Eu was best fitted to a biexponential function (Figure S6B), and the corresponding average lifetimes, $\langle\tau_{av}\rangle$, are summarized in Table S3. Here, the BSA fluorescence lifetime remained unaltered upon addition of 1·Eu, indicating that the quenching follows a static mechanism. The formation of a ground-state complex between BSA and 1·Eu was further confirmed by the appearance of a weakly absorbing band/shoulder in the UV–visible absorption spectrum of BSA at around 320–330 nm (see Figure S6C). This band was also

observed in the excitation spectra, recorded at the Eu(III) $^5D_0 \rightarrow {}^7F_2$ transition (616 nm), of 1·Eu in the presence of increasing amounts of BSA.

The same behavior was also observed in both the steady state and the time-resolved fluorescence measurements, when such titrations were carried out, where increasing amounts of AuNP-1·Eu were added to a solution of BSA (7.5 μM) (see Table S3 and Figure S7). Again, here, the excitation spectra were monitored at 616 nm and showed the appearance of the same band around 330 nm, clearly indicating the sensitization of the Eu(III) emission by the protein chromophores (*e.g.*, essentially tryptophan), in the absence of nta (Figure S7B). As the quenching was shown to be purely static, the fluorescence data were analyzed using the modified Stern–Volmer equation (see eq 1, Experimental Section) to determine the binding constant of 1·Eu with BSA,[64] which is directly obtained from the linear regression when $F_0/(F_0 - F)$ is plotted against $[Q]^{-1}$, as shown in Figure S6A, where the binding constant log K was determined as 4.3 ± 0.3 for this interaction. This binding constant, while corresponding to the values determined for similar cyclen chelates,[57,58] is particularly interesting, as it is of the same order of magnitude as the binding (association constant) of a wide range of drugs, or small organic molecules, with serum albumin.[65,66] This result was further confirmed by analyzing the changes in the UV–visible titration of BSA with 1·Eu using the nonlinear regression analysis program SPECFIT,[67,68] which yielded log K = 4.9 ± 0.1 (Figure S6C). On the other hand, the binding constant of 1·Eu with nta has been determined, by both linear and nonlinear regression analysis, to be log $K \approx$ 8.6 ± 0.3 and 8.8 ± 0.6, respectively (see Figure S8 and eq 2). Consequently, according to these binding results, the quenching of the Eu(III) emission observed earlier for the AuNP-1·Eu-nta system upon addition of BSA (Figure 3) is more likely to be the result from an antenna–protein (nta–BSA) interaction, rather than a displacement of the nta from the Eu(III) first coordination sphere by the protein. This assumption was further strengthened by the significant decrease in the average fluorescence lifetime of BSA once nta was added to both the BSA-1·Eu and the BSA-AuNP-1·Eu systems, as shown in Figures S6B and S7B, respectively.

Unraveling the BSA–nta Interaction. In order to further investigate the interaction between the nta antenna and the protein, as well as the mechanism of the quenching of the Eu(III) emission, both steady-state and time-resolved fluorescence measurements were carried out using the simple nta–BSA system. These measurements showed that the addition of nta to a solution of BSA gave rise to complete quenching of the protein fluorescence. However, no shift in the emission maximum was observed (Figure 5), indicating that the interaction between nta and BSA did not alter the local

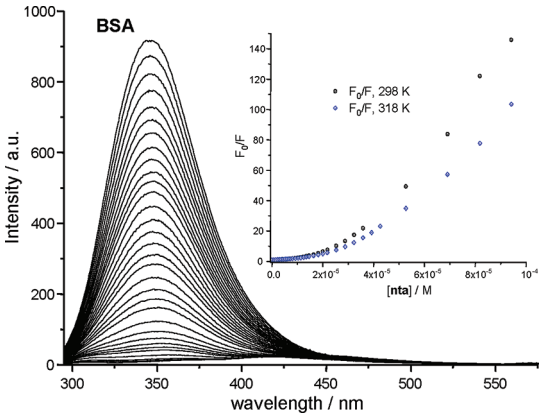

Figure 5. Observed quenching of the BSA fluorescence (λ_{ex} = 280 nm) upon addition of increasing amounts of nta in Hepes buffer (pH 7.4) at 298 K. Inset: Resulting Stern–Volmer plots (F_0/F *vs* [nta]) at two temperatures (298 and 318 K); [BSA] = 7.5 × 10^{-6} M and [nta] = (0→9.41) × 10^{-5} M.

dielectric environment of the fluorescent amino acid residues in the protein. The fluorescence quenching data were analyzed using the Stern–Volmer method (see eq 3), and the resulting Stern–Volmer plots, at two different temperatures (T = 298, 318 K), are shown as an inset in Figure 5. Taking into the account the concentration range (0→4) × 10^{-6} M, where the Stern–Volmer plots remained linear, average quenching constants K_{SV} were estimated as 8.80 × 10^4 and 8.29 × 10^4 M^{-1} at 298 and 318 K, respectively. The decrease in K_{SV} with increasing temperature clearly indicated the presence of static quenching. However, the upward curvature of the plots strongly suggested that both static and dynamic quenching are occurring for this system.[63] The dynamic quenching contribution was confirmed by measuring the fluorescence lifetimes of BSA in Hepes buffer in the absence and presence of nta, where the BSA fluorescence lifetime was best fit to a biexponential function, yielding an average lifetime of 6.35 ± 0.03 ns, which is in agreement with that reported by Togashi *et al.*[69] When nta was added to this protein solution, the decay profiles were no longer found to be biexponential, but best fit to a triexponential function, where the average fluorescence lifetimes ($\langle\tau_{av}\rangle$) were significantly shortened, giving $\langle\tau_{av}\rangle$ = 5.42 ns once one equivalent of nta was added. The decrease in the BSA lifetimes as the concentration of nta was increased (see Table S4) confirmed the occurrence of a dynamic quenching process for this system. These changes were analyzed using eq 3, from which the quenching constants K_{SV} and k_q were estimated as (2.36 ± 0.04) × 10^4 M^{-1} and (3.7 ± 0.1) × 10^{12} $M^{-1}\cdot s^{-1}$, respectively (see Figure S9A), demonstrating that the bimolecular quenching rate constant was 2 orders of magnitude higher than the value for maximum scattering collision quenching constant with biopolymer (k_q = 2.0 × 10^{10} $M^{-1}\cdot s^{-1}$) and thus suggesting that the excited state of the protein is affected not only by

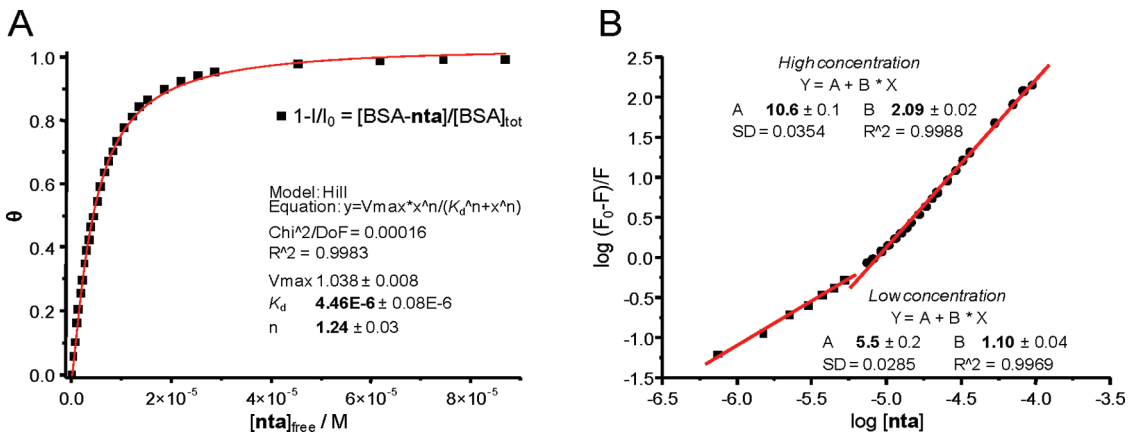

Figure 6. (A) Saturation binding curve of BSA as a function of the concentration of free nta and the resulting fit using the Hill equation. (B) Double-log plot of nta quenching effect on the BSA fluorescence and the resulting linear fits; [BSA] = 7.5 × 10^{-6} M in both cases.

collisional quenching. Indeed, fluorescence resonance energy transfer from the protein to the diketonate is expected to take place as well, considering the large overlap between the BSA fluorescence and the absorption of nta (Figure S9B). Since dynamic quenching affects only the excited states of the fluorophores, the presence of static quenching and thus formation of a ground-state complex between BSA and nta were further ascertained from UV−visible spectroscopic studies (Figure S10). Upon addition of BSA, the lower energy absorption band of nta at 330 nm displayed a marked hypsochromic shift of 8 nm, with a concomitant decrease of 10% in absorbance. The difference absorption spectrum (curve 4, Figure S10B) obtained by subtracting the absorption spectrum of nta from the one obtained for BSA−nta at the same concentration clearly demonstrated the presence of static quenching, the existence of a negative band indicating that the absorption spectrum of BSA−nta does not overlap with the sum of the absorption spectra of nta and BSA.

The binding constants of the ground-state complexes formed between BSA and nta were determined using both linear and nonlinear least-squares analysis, by globally fitting the changes in the absorption and the emission spectra. The fluorescence data were first analyzed using the Hill equation, eq 4, Experimental Section,[70] by plotting the fractional saturation of the protein as a function of the quencher concentration (in this case, nta), resulting in the saturation binding curve, shown in Figure 6A. This allowed for the determination of an average binding constant log K as 5.35 ± 0.02. The Hill coefficient, n_H, representing the degree of cooperativity of the binding, was found to be n_H = 1.24, indicative of positive cooperativity. To further ascertain this, the Hill equation was linearized to obtain eq 5, which has been used to determine the number of binding sites (n) as well as the individual binding constants. The resulting double-logarithm plot (Figure 6B) displayed two distinct linear regressions, depending on the ligand concentration range, which are characteristic of a multisite cooperative binding event. At low nta concentration, a slope close to unity was obtained, indicating the presence of a single binding site for nta with a binding constant log K_{11} = 5.5 ± 0.2. When reaching higher nta concentrations, the slope of the linear fit indicated the presence of two binding sites, from which the binding constant for the formation of the 1:2 BSA:nta complex was estimated to be log β_{12} = 10.6 ± 0.1 (a log K_{12} value of 5.1).

The formation of two different species in solution was further confirmed by the method of continuous variation (Job's plot analysis) and by fitting both the nta-induced BSA fluorescence quenching data and the changes observed in the UV−visible absorption titration of nta with BSA, using the nonlinear regression analysis program SPECFIT (Figure S11). The binding constants obtained from these different fitting procedures are summarized in Table 1.

Since the nta-induced fluorescence quenching of the protein was highly effective, it was assumed that the nta molecules were interacting and thus quenching both of the Trp fluorophores, independently from their location (*e.g.*, Trp-134 is located on the protein surface, while Trp-212 is buried inside the protein structure). This assumption was confirmed by recording the ^{19}F NMR spectrum of the nta in the absence and presence of the protein. The spectrum of a 470 μM nta solution in phosphate buffer displayed two main resonances at −75.3 and −85.6 ppm, corresponding to the enol and keto forms, respectively (Figure S12). The addition of one equivalent of BSA led to a significant broadening of these resonances, appearing as a set of three resonances, between −72 and −76 ppm. The aforementioned broadening is a clear indication that nta was able to penetrate inside the protein structure and interact with the Trp-212 residue. This would result in direct change in the intrinsic fluorescence of the Trp-212 residue, which we indeed observed in our

TABLE 1. Binding Constants for the BSA−nta System in Buffered Solution (pH 7.4, T = 298 K) Obtained Using Linear and Nonlinear Fitting Procedures

		nonlinear			linear
method (spectroscopic data)		Hill method (fluorescence)	SPECFIT (fluorescence)	SPECFIT (UV−vis)	double log (fluorescence)
log β (BSA:nta)	1:1	5.35 ± 0.02	5.64 ± 0.04	5.8 ± 0.2	5.5 ± 0.2
	1:2		10.82 ± 0.04	11.2 ± 0.2	10.6 ± 0.1

investigations discussed above. Furthermore, when 6 M guanidine hydrochloride, a common protein denaturant, was added to the NMR sample, the two main signals, initially observed at −75.3 and −85.6 ppm, respectively, were reinstated (see Figure S12). However, a small downfield shift of the keto peak from its original position, considered as arising from a change in susceptibility due to the addition of 6 M guanidine hydrochloride, was observed.[71]

Having quantified the binding affinity between nta and BSA and shown the ability of nta to reach the interior of the protein, it was important to investigate to what extent the conformation and/or microenvironment of BSA are affected upon binding. Synchronous fluorescence spectroscopy is often employed to provide information about the molecular environment in the vicinity of fluorophores. In proteins, characteristic synchronous fluorescence of tyrosine and tryptophan residues are obtained when $\Delta\lambda$ is set as 15 and 60 nm, respectively.[72,73] Synchronous fluorescence spectral changes of BSA upon addition of increasing amounts of nta are shown in Figure S13A, where the λ_{Fmax} of the protein was slightly blue-shifted (∼1−2 nm) when $\Delta\lambda$ was set as 15 nm, while remaining unchanged when $\Delta\lambda$ = 60 nm. The blue-shift observed was attributed to a minor change in the polarity of the microenvironment around the tyrosine residue, but the polarity around the tryptophan residues did not seem to be affected by the binding process. However, the similar quenching percentages of fluorescence intensity for tyrosine and tryptophan implied that the binding site of nta should be located in the vicinity of both amino acids. To further investigate whether any conformational changes occurred in the structure of BSA upon binding of nta, circular dichroism (CD) experiments were carried out, and these showed that the CD spectrum of BSA exhibited a strong negative ellipticity at 209 and 222 nm, characteristic for a protein with a predominant α-helix structure.[73−75] The CD spectra of BSA in the absence and presence of nta were similar in shape and thus indicated that the binding of nta did not affect considerably the BSA secondary structure, the latter remaining predominantly α-helical. To confirm this, secondary structure analysis showed a small 1.0% reduction of α-helical structures at a 1:4 molar ratio of BSA to nta, while for a higher 1:8 or 1:16 ratio, typically encountered in our full system, a 1.5% and 1.8% decrease in the α-helical content are observed for these ratios, respectively (see Figure S13B). These results demonstrate that the BSA does not undergo significant conformational changes upon interacting with nta, which is important for the use of this system, for instance in sensing applications, as it indicates that tertiary interactions such as those occurring between proteins or protein−drugs would not be affected by the presence of the nta.

Use of AuNP-1·Eu As Luminescent Reporter for the Binding of Drugs to BSA. The investigation performed on the nta−BSA system clearly demonstrated the existence of a strong interaction between the protein and nta, while the binding does not lead to structural changes within the protein. This interaction has been assumed to be at the origin of the Eu(III) emission quenching observed previously when AuNP-1·Eu-nta was titrated with BSA, as shown in Figure 3. With this in mind, we foresaw that the Eu(III) emission could act as an impartial reporter, which could be used to observe the interaction between the protein and substrates, regardless of all the intermediate energy transfer and/or quenching processes that can occur as a consequence of the formation of a protein:substrate assembly; that is, the emission arising from AuNP-1·Eu-nta could be used to signal such reversible interactions. To verify this hypothesis, the quenching of the Eu(III) emission observed upon binding of nta to BSA was analyzed using eq 1. The binding constant obtained from the linear regression analysis of these changes gave log K = 5.06 ± 0.03, which is close to the binding constant obtained in our analysis above, Table 1. This suggests that the nta−BSA binding event is the main contributor to the quenching of the Eu-centered emission, confirming the above hypothesis.

Taking advantage of such nta−BSA interaction, we used this self-assembly as a sensing tool for observing the binding of small molecules, such as drugs and toxins, to serum albumin. Here the AuNP-1·Eu-nta−BSA system would function as a displacement self-assembly unit, where the drug would compete with nta for binding to the protein, partially or completely displacing the antennae from the protein structure. This would result in concomitant changes in the photophysical properties of the AuNP-1·Eu-nta system, which would be directly correlated to the concentration of the competing analyte. We thus next

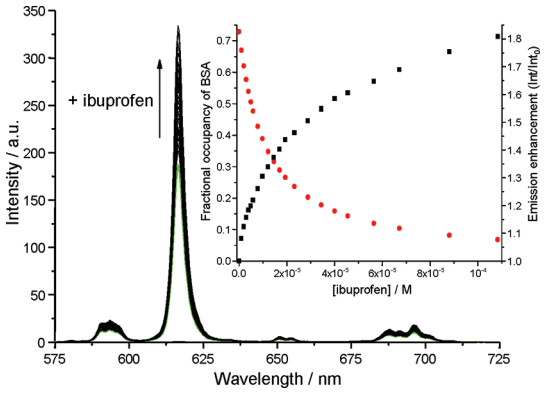

Figure 7. Evolution of the Eu(III) emission of AuNP-1·Eu-nta in the presence of BSA (BSA:nta in a 1:1 ratio) upon titration with ibuprofen ((0→1.08) × 10^{-4} M) in Hepes buffer (pH 7.4). Inset: Fractional occupancy of BSA by nta (red circles) and the emission enhancement (squares) observed for the integrals of the Eu(III) $^5D_0/^7F_2$ transition as a function of the concentration of ibuprofen added.

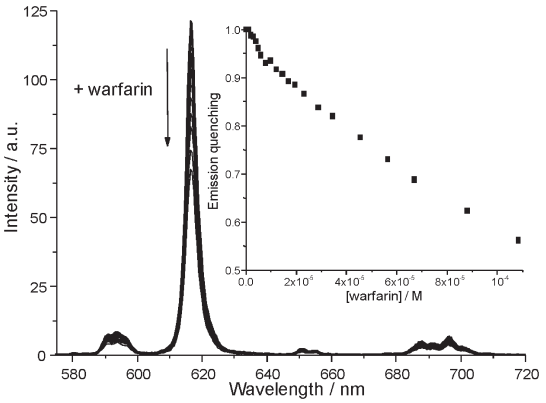

Figure 8. Evolution of the Eu(III) emission of AuNP-1·Eu-nta in the presence of BSA (BSA:nta in a 1:1 ratio) upon titration with warfarin ((0→1.08) × 10^{-4} M) in Hepes buffer (pH 7.4). Inset: Changes in the Eu(III) $^5D_0 \rightarrow ^7F_2$ emission integrals calculated as a function of the concentration of warfarin added.

carried out competitive titrations, where the Eu(III) emission of the AuNP-1·Eu-nta system bound to BSA was measured upon addition of a specific competitor, such as ibuprofen, a well-known BSA site II (subdomain IIIA) marker.[66,76,77] The overall changes in the Eu(III) emission of AuNP-1·Eu-nta−BSA upon titration with ibuprofen ((0→1.08) × 10^{-4} M, 0 → 10 equivalents) are shown in Figure 7, demonstrating that the emission was enhanced by *ca.* 1.8-fold. Despite the enhancement, the metal-centered emission was, however, not fully recovered from the initial 75% quenching resulting from the binding of AuNP-1·Eu-nta to BSA (nta:BSA 1:1). Hence, these results demonstrate that ibuprofen only partially displaces the antenna, but to a measurable extent. The fractional occupancy (*f*) of the protein by nta in the presence of ibuprofen was calculated using eq 6, and the results are shown in Figure 7, together with the total Eu(III) emission enhancement. The inset in Figure 7 clearly demonstrates that as soon as *f* decreased, a concomitant enhancement was observed in the metal-centered luminescence, which can be viewed as a direct consequence of the competitive drug−BSA interaction, where the emission enhancement occurs mainly within the μM concentration range, reaching saturation at >0.1 mM concentrations of the drug.

To confirm that the binding of ibuprofen, and thus the concomitant displacement of the antenna occurring, several additional spectroscopic experiments were undertaken. The normalized excitation spectra, when recorded at 616 nm (Eu(III) $^5D_0 \rightarrow ^7F_2$ transition), were shown to be fully superimposable throughout the course of the titration, indicating that the Eu(III) emission enhancement was due to a more efficient sensitization of the Eu(III) by nta and not from an additional energy transfer involving ibuprofen (Figure S14). Displacement of the protein from the nta antenna was also confirmed by UV−visible absorption spectroscopy, where upon the addition of ibuprofen, the low-energy absorption band of nta at 332 nm, which was initially blue-shifted by *ca.* 14 nm by the addition of BSA, was red-shifted, almost recovering its initial (free) position once 10 equivalents of ibuprofen were added (see Figure S15). The same series of measurements were performed with site I (subdomain IIA) marker warfarin.[66,76,77] Addition of the latter to a solution of AuNP-1·Eu-nta containing BSA (in 1:1 nta:BSA ratio) did not result in any enhancement in the Eu(III) emission. On the contrary, a steady decrease was observed in the Eu(III) emission intensity, as shown in Figure 8.

The further quenching of the metal-centered emission upon addition of warfarin was attributed to the strong absorption of the coumarin-based drug (λ_{max} = 309 nm, ε_{309} = 13591 ± 82 $M^{-1}\cdot cm^{-1}$) in the absorption range of the nta antenna (Figure S16), resulting in an alteration of its sensitization efficiency. The excitation spectra, recorded at 616 nm (Eu(III) $^5D_0 \rightarrow ^7F_2$ transition) and normalized at the 340 nm maximum, showed a continuous intensity decrease for all excitation wavelengths lower than 335 nm, as a result of the strong warfarin absorption in the 300−340 nm range (Figure S17). Indeed, the relative decrease at both 309 and 330 nm in the excitation spectrum matched, within the experimental error, the relative increase in the absorption spectrum at the same wavelengths (see Figure S18). However, when the excitation was performed at 345 nm (instead of 330 nm, to avoid the warfarin absorption band), a similar quenching in the Eu(III) emission was observed, indicating that an alternative quenching pathway was operational. A possible explanation for this would involve a conformational change in the protein structure upon binding of warfarin in site I, consequently, leading to a slight modification in the nta−BSA binding/interaction. Even if this is the case, these results demonstrate that the warfarin and nta do not share a common binding site

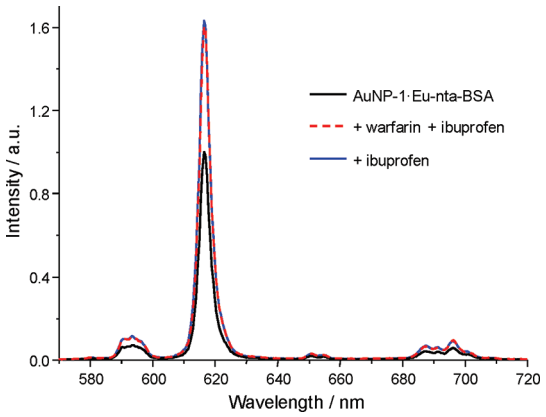

Figure 9. Eu-centered emission enhancement observed for AuNP-1·Eu-nta−BSA (black, —) upon addition of ibuprofen alone (blue, —) or warfarin + ibuprofen (red, ---) in Hepes-buffered solution (pH 7.4).

within the structure of BSA. On the contrary, ibuprofen has been shown to compete with nta for binding to BSA, and therefore nta has been located in the same binding site as ibuprofen, namely, site II. Interestingly, the presence of warfarin in the site I of BSA has no, or little, influence on the detection of the site II drug, as shown in Figure 9. Indeed, the luminescent Eu(III) enhancement factor upon addition of 5 equivalents of ibuprofen (1.65) remained identical, within experimental error, even in the presence of 10 equivalents of warfarin (1.60).

CONCLUSIONS

In this article, the photophysical properties of the luminescent AuNP-1·Eu-nta, obtained through the self-assembly, taking place at the gold surface, between the Eu·1 cyclen complex and the sensitizing naphthalene β-diketone antenna, nta, were investigated in the presence of the protein BSA. Using TEM and DLS analyses we confirmed the stability of the AuNP-1·Eu in water over a long period, as no NP aggregation was observed, which was further ascertained by the position of the SPR absorption band. The Eu(III)-centered emission was shown to be greatly enhanced by the addition of nta due to the efficient sensitization of the Eu($^5D_0$) excited state. This emission enhancement was used to estimate the number of Eu·1 complexes attached at the surface of each AuNP, which was found to be *ca.* 120. When BSA was added to a solution of AuNP-1·Eu-nta, a significant quenching of the metal-centered was observed. The evolution observed in the excitation spectrum of AuNP-1·Eu-nta and the binding constants determined for the formation of the self-assembly between Eu·1 and nta, as well as between Eu·1 and BSA, demonstrated that a displacement of nta from the Eu(III) first coordination sphere by BSA was not possible. Moreover, a complete photophysical investigation including fluorescence quenching and time-resolved measurements was carried out on the simple nta−BSA system and showed that a strong interaction took place between the protein and the nta antenna. In addition to the fluorescence measurements, the information obtained from ^{19}F NMR experiments brought evidence for the nta penetrating the interior of BSA without, however, resulting in a sizable perturbation of the protein secondary structure, as demonstrated by SFS and CD spectroscopic techniques. The modulation observed in the Eu(III) emission upon addition of BSA to the AuNP-1·Eu-nta was analyzed, and the binding constant determined was found to be in good agreement with that obtained from the fluorescence quenching data, indicating that the AuNP-1·Eu-nta system can function as an accurate reporter for the binding/interaction of small molecules with proteins, regardless of all the different energy transfer and/or quenching processes taking place prior to reaching the Eu(III) excited state. This finding was applied further for the detection of universal drugs, where the partially "switched off" AuNP-1·Eu-nta−BSA system was "switched on" again upon addition of a competitive drug, *i.e.*, ibuprofen. The competitive titrations carried out with both site I (warfarin) and site II markers (ibuprofen) allowed the localization of nta within the binding site II of BSA. Interestingly, the presence of a site I drug did not affect the detection of a site II drug, in this case ibuprofen. In conclusion, the system designed and studied in the present article demonstrates the successful combination of the unique properties of both lanthanides and AuNPs within the view of developing promising nanomaterials that will find numerous applications in the biomedical fields, as sensors and/or imaging agents.

EXPERIMENTAL SECTION

Materials and Methods. All solvents and chemicals were purchased from commercial sources and used without further purification. Water was purified using a Millipore Milli-Q water purification system. BSA (fraction V, ≥96%), nta (4,4,4-trifluoro-1-(2-naphthyl)-1,3-butanedione, 99%), ibuprofen (2-(4-isobutylphenyl)propionic acid, > 98.0%), and HEPES buffer (titration, ≥99.5%) were from Fluka, Aldrich, TCI, and Sigma, respectively. The HEPES buffer solution was prepared by dissolving 4-(2 hydroxyethyl)piperazine-1-ethanesulfonic acid (HEPES, 0.1 M) and NaCl (ionic strength) in Millipore water before the pH was adjusted to 7.4 with NaOH. ^{19}F NMR (376.6 MHz) spectra were recorded using a Bruker Spectrospin DPX-400 spectrometer. The samples were measured in 10 mM phosphate buffer.

Characterization of the Surface-Modified AuNPs. The size of the functionalized AuNP and their distribution in aqueous solution were determined by transmission electron microscopy and dynamic light scattering, respectively. TEM analyses were

carried out at the Centre for Microscopy and Analysis (CMA, Trinity College Dublin) using a JEOL 2100 microscope. DLS measurements were performed on (1−3) × 10^{-7} M solutions of AuNP in distilled water using a Zetasizer Nano Series (Malvern Instruments). The number of Eu(III) cyclen complexes attached to the AuNP has been determined by measuring the changes in the Eu(III)-centered emission when a 10^{-7} M solution of AuNP-1·Eu was titrated with nta. The maximum emission observed corresponded to the saturation of the Eu(III) first coordination sphere of each cyclen complex present on the AuNP surface. Therefore, knowing that nta forms 1:1 ternary complexes with 1·Eu, the number of equivalents of nta required to reach the maximum emission enhancement has been considered as a reasonable approximation for the number of cyclen complexes attached to each AuNP.

Photophysical Measurements. Unless otherwise stated, all measurements were performed at 298 K in Hepes buffer at pH 7.4, while the ionic strength was kept constant by the addition of NaCl (0.1 M). UV−visible absorption spectra were measured in 1 cm quartz cuvettes on a Varian Cary 50 spectrophotometer. Baseline correction was applied for all spectra. Emission (fluorescence, phosphorescence, and excitation) spectra and lifetimes were recorded on a Varian Cary Eclipse fluorimeter. Quartz cells with a 1 cm path length from Hellma were used for these measurements. The temperature was kept constant throughout the measurements by using a thermostatted unit block. CD spectra of BSA in the absence and presence of nta were recorded with a JASCO J-810 spectropolarimeter using a quartz cell with a path length of 0.4 cm. Three scans were accumulated at a scan speed of 50 nm·min^{-1}, with data being collected every 0.5 nm from 200 to 300 nm. For CD studies, the BSA solution was prepared in 10 mM phosphate buffer at a concentration of 1.5 × 10^{-6} M. Prediction of the secondary structure was derived by deconvoluting the data sets by a neural approach[78] using the CDNN 2.1 program. Synchronous fluorescence spectra of BSA in the absence and presence of different amounts of nta were measured with $\Delta\lambda$ = 15 and 60 nm on a Fluorolog FL 3-22 spectrophotometer from Horiba Jobin Yvon.

Spectrophotometric Titrations and Binding Parameters. In a typical experiment, 120 equivalents of nta were added prior to titration to a 2.7 mL HEPES-buffered solution of 10^{-7} M AuNP-1·Eu. The resulting solution was then titrated with BSA (0−675 equivalents). After each BSA addition, UV−visible, fluorescence, phosphorescence, and excitation spectra as well as the Eu($^5D_0$) excited-state lifetimes were recorded at 298 K. Fluorescence quenching of BSA in the presence of 1·Eu was measured at 298 K, and the data collected were analyzed using the modified Stern−Volmer equation:[63,64]

$$\frac{F_0}{F_0 - F} = \frac{1}{f_a} + \frac{1}{f_a K_a}\frac{1}{[Q]} \quad (1)$$

where f_a represents the fraction of the initial fluorescence accessible to the quencher; F and F_0 are the fluorescence of BSA in the presence and absence of the quencher, respectively. The binding constant, K_a, for the complex formation between BSA and 1·Eu was then given by the inverse of the slope multiplied by the ordinate at the origin (f_a^{-1}). Factor analysis and mathematical treatment of the UV−visible spectra were performed with the SPECFIT program.[67,68] Spectrophotometric titrations of 1·Eu (10^{-5} M) with nta were also performed, and the data obtained were fitted using SPECFIT as well as eq 2 to determine the binding constant K for the interaction between nta and 1·Eu:[79]

$$\log\left(\frac{F - F_{min}}{F_{max} - F}\right) = \log K_a + n \log[\text{nta}] \quad (2)$$

where F is the emission intensity, F_{min}, the minimum emission intensity at zero [nta], and F_{max}, the maximum emission intensity at saturating [nta], *i.e.*, when each 1·Eu formed a ternary complex with nta.

Quenching experiments with nta were conducted at both 298 and 318 K. The quenching processes between the protein and nta were first analyzed using the Stern−Volmer equation:[63]

$$\frac{F_0}{F} = \frac{\tau_0}{\tau} = 1 + K_{SV}[Q] = 1 + k_q\tau_0[Q] \quad (3)$$

where K_{SV} represents the Stern−Volmer quenching constant, which is defined as the product of k_q, the bimolecular quenching rate constant, and τ_0, the BSA fluorescence lifetime in the absence of quencher.

The binding constant for the association between nta and BSA was determined by fitting the data collected according to the saturation binding model using the Hill equation:[70]

$$\Theta = \frac{y}{1 - y} = \frac{B_{max}[Q]^{n_H}}{K_d{}^{n_H} + [Q]^{n_H}} \quad (4)$$

where Θ represents the fractional saturation of the protein, namely, the fraction or percent of protein to which the ligand is bound, and B_{max} is the maximum amount of the complex BSA−nta formed at saturation of the ligand. Plotting Θ as a function of the free nta concentration in solution allows the determination of the equilibrium dissociation constant K_d (defined as $1/K_a$) and n_H, the Hill coefficient.

The number of binding sites (n) per BSA and the individual binding constants were evaluated from the linear double-logarithm plot:[64]

$$\log\left(\frac{F_0 - F}{F}\right) = \log K_a + n \log[Q] \quad (5)$$

The binding constants obtained were further ascertained by fitting both absorption and fluorescence data with SPECFIT.

Competitive Titrations. In order to identify the binding sites of nta on BSA and investigate the potential of our system as a drug sensor, warfarin and ibuprofen were used as the markers for sites I and II, respectively. In a typical experiment, the ratio of nta:BSA was kept at 1:1, while the concentration of the marker was progressively increased from 0 to 10 equivalents ((0→1.08) × 10^{-4} M). After each addition, the absorption and emission spectra were measured as previously described. The data collected were analyzed using the agonist−antagonist model, which describes the receptor (BSA) occupancy by agonist (nta) in the presence of a competitive antagonist (ibuprofen):

$$f = \frac{[A]}{[A] + K_d^a\left(1 + \frac{[B]}{K_d^b}\right)} \quad (6)$$

where [A] and [B] are the concentrations of the nta and ibuprofen, respectively and K_d is their dissociation constant.[80] The fractional occupancy was calculated using the average dissociation constant determined using the Hill equation for nta (log K = 5.35, K_d = 4.47 × 10^{-6} M), while that of ibuprofen was taken from the literature (log K = 5.52, K_d = 3.02 × 10^{-6} M).[66]

Time-Resolved Luminescence Measurements. Phosphorescence lifetimes of the Eu($^5D_0$) excited state were measured in time-resolved mode throughout the titration with BSA. They are averages of three independent measurements, which were made by monitoring the emission decay at 616 nm, which corresponds to the maxima of the Eu(III) $^5D_0 \rightarrow {}^7F_2$ transition, enforcing a 0.1 ms delay. Both mono- and biexponential decays were analyzed using Origin 7.5.

Fluorescence lifetime measurements were performed with a Horiba Jobin Yvon Fluorolog FL 3-22 equipped with a FluoroHub v2.0 single-photon controller using the time-correlated single-photon counting method, run in reverse mode. The sample solutions were excited at 261 nm with a pulsed nanosecond light-emitting diode (NanoLED). The time distribution of the lamp pulse (<1.0 ns), also called the instrument response function, was recorded prior to lifetime measurements in a separate experiment using a scatter solution, in this case a solution of Ludox (Aldrich). All the measurements were performed at 298 K.

The decays were analyzed using IBH DAS6 software, and the data fitted as a sum of exponentials, employing a nonlinear

least-squares error minimization analysis:

$$I(t) = \sum_{i=1}^{n} \alpha_i \exp\left(\frac{-t}{\tau_i}\right) \quad (7)$$

The pre-exponential factors (α_i) are shown normalized, and the errors are taken as two standard deviations. The goodness of the fit was assessed by the chi-squared value as well as the symmetric distribution of the residuals about the zero axes. The average lifetime $\langle\tau\rangle$ is given by[63]

$$\langle\tau\rangle = \frac{\sum \alpha_i \tau_i^2}{\sum \alpha_i \tau_i} = \sum f_i \tau_i \quad (8)$$

where the fractional contribution of the lifetime i, f_i, is defined as $f_i = \alpha_i\tau_i/\Sigma_j\alpha_j\tau_j$.

Acknowledgment. The authors thank Science Foundation Ireland (RFP 2008 and 2009), The Irish Research Council for Science, Engineering & Technology (IRCSET), and Swiss National Science Foundation (SNSF) (S.C.) for funding, Dr. Julien Massue for helping with the initial formation of the NPs, and Dr. Oxana Kotova for helpful discussions. We also thank Dr. John O'Brien for technical assistance and helpful discussions regarding the ^{19}F NMR experiments.

Supporting Information Available: Theoretical MM2 calculations for the size characterization of the AuNP-1·Eu system and details on the photophysical investigations for each system studied, including lifetime tables, absorption, fluorescence, phosphorescence, and excitation spectra, as well as the different fits performed to determine quenching and/or binding constants. This material is available free of charge *via* the Internet at http://pubs.acs.org.

REFERENCES AND NOTES

1. Rosi, N. L.; Mirkin, C. A. Nanostructures in Biodiagnostics. *Chem. Rev.* **2005**, *105*, 1547–1562.
2. Jarzyna, P. A.; Gianella, A.; Skajaa, T.; Knudsen, G.; Deddens, L. H.; Cormode, D. P.; Fayad, Z. A.; Mulder, W. J. M. Multifunctional Imaging Nanoprobes. *Wiley Interdiscip. Rev.: Nanomed. Nanobiotechnol.* **2010**, *2*, 138–150.
3. Zrazhevskiy, P.; Sena, M.; Gao, X. Designing Multifunctional Quantum Dots for Bioimaging, Detection, and Drug Delivery. *Chem. Soc. Rev.* **2010**, *39*, 4326–4354.
4. Adair, J. H.; Parette, M. P.; Altinoglu, E. I.; Kester, M. Nanoparticulate Alternatives for Drug Delivery. *ACS Nano* **2010**, *4*, 4967–4970.
5. Shi, J.; Votruba, A. R.; Farokhzad, O. C.; Langer, R. Nanotechnology in Drug Delivery and Tissue Engineering: From Discovery to Applications. *Nano Lett.* **2010**, *10*, 3223–3230.
6. Bhattacharya, R.; Mukherjee, P. Biological Properties of "Naked" Metal Nanoparticles. *Adv. Drug Delivery Rev.* **2008**, *60*, 1289–1306.
7. Rivera Gil, P.; Parak, W. J. Composite Nanoparticles Take Aim at Cancer. *ACS Nano* **2008**, *2*, 2200–2205.
8. Bechet, D.; Couleaud, P.; Frochot, C.; Viriot, M. L.; Guillemin, F.; Barberi-Heyob, M. Nanoparticles as Vehicles for Delivery of Photodynamic Therapy Agents. *Trends Biotechnol.* **2008**, *26*, 612–621.
9. Wan, A. C. A.; Ying, J. Y. Nanomaterials for *in Situ* Cell Delivery and Tissue Regeneration. *Adv. Drug Delivery Rev.* **2010**, *62*, 731–740.
10. Sperling, R. A.; Rivera gil, P.; Zhang, F.; Zanella, M.; Parak, W. J. Biological Applications of Gold Nanoparticles. *Chem. Soc. Rev.* **2008**, *37*, 1896–1908.
11. Zhao, Y.; Tian, Y.; Cui, Y.; Liu, W.; Ma, W.; Jiang, X. Small Molecule-Capped Gold Nanoparticles as Potent Antibacterial Agents That Target Gram-Negative Bacteria. *J. Am. Chem. Soc.* **2010**, *132*, 12349–12356.
12. Rosi, N. L.; Giljohann, D. A.; Thaxton, C. S.; Lytton-Jean, A. K. R.; Han, M. S.; Mirkin, C. A. Oligonucleotide-Modified Gold Nanoparticles for Intracellular Gene Regulation. *Science* **2006**, *312*, 1027–1030.
13. Wang, Z.; Ma, L. Gold Nanoparticle Probes. *Coord. Chem. Rev.* **2009**, *253*, 1607–1618.
14. Lisowski, C. E.; Hutchison, J. E. Malonamide-Functionalized Gold Nanoparticles for Selective, Colorimetric Sensing of Trivalent Lanthanide Ions. *Anal. Chem.* **2009**, *81*, 10246–10253.
15. Liu, R. R.; Liew, R. S.; Zhou, H.; Xing, B. G. A Simple and Specific Assay for Real-Time Colorimetric Visualization of Beta-Lactamase Activity by Using Gold Nanoparticles. *Angew. Chem., Int. Ed.* **2007**, *46*, 8799–8803.
16. Lin, Y. W.; Huang, C. C.; Chang, H. T. Gold Nanoparticle Probes for the Detection of Mercury, Lead and Copper Ions. *Analyst (Cambridge, U. K.)* **2011**, *136*, 863–871.
17. Dulkeith, E.; Ringler, M.; Klar, T. A.; Feldmann, J.; Muñoz Javier, A.; Parak, W. J. Gold Nanoparticles Quench Fluorescence by Phase Induced Radiative Rate Suppression. *Nano Lett.* **2005**, *5*, 585–589.
18. Mayilo, S.; Kloster, M. A.; Wunderlich, M.; Lutich, A.; Klar, T. A.; Nichtl, A.; Kürzinger, K.; Stefani, F. D.; Feldmann, J. Long-Range Fluorescence Quenching by Gold Nanoparticles in a Sandwich Immunoassay for Cardiac Troponin T. *Nano Lett.* **2009**, *9*, 4558–4563.
19. Lu, Y.; Dasog, M.; Leontowich, A. F. G.; Scott, R. W. J.; Paige, M. F. Fluorescently Labeled Gold Nanoparticles with Minimal Fluorescence Quenching. *J. Phys. Chem. C* **2010**, *114*, 17446–17454.
20. Thomas, K. G.; Kamat, P. V. Chromophore-Functionalized Gold Nanoparticles. *Acc. Chem. Res.* **2003**, *36*, 888–898.
21. Anger, P.; Bharadwaj, P.; Novotny, L. Enhancement and Quenching of Single-Molecule Fluorescence. *Phys. Rev. Lett.* **2006**, *96*, 113002-1–113002-4.
22. Jennings, T. L.; Singh, M. P.; Strouse, G. F. Fluorescent Lifetime Quenching Near d=1.5 nm Gold Nanoparticles: Probing NSET Validity. *J. Am. Chem. Soc.* **2006**, *128*, 5462–5467.
23. Gunnlaugsson, T.; Leonard, J. P. Responsive Lanthanide Luminescent Cyclen Complexes: From Switching/Sensing to Supramolecular Architectures. *Chem. Commun.* **2005**, 3114–3131.
24. Bünzli, J.-C. G.; Comby, S.; Chauvin, A.-S.; Vandevyver, C. D. B. New Opportunities for Lanthanide Luminescence. *J. Rare Earths* **2007**, *25*, 257–274.
25. dos Santos, C. M. G.; Harte, A. J.; Quinn, S. J.; Gunnlaugsson, T. Recent Developments in the Field of Supramolecular Lanthanide Luminescent Sensors and Self-Assemblies. *Coord. Chem. Rev.* **2008**, *252*, 2512–2527.
26. Bünzli, J.-C. G. Lanthanide Luminescence for Biomedical Analyses and Imaging. *Chem. Rev.* **2010**, *110*, 2729–2755.
27. Montgomery, C. P.; Murray, B. S.; New, E. J.; Pal, R.; Parker, D. Cell-Penetrating Metal Complex Optical Probes: Targeted and Responsive Systems Based on Lanthanide Luminescence. *Acc. Chem. Res.* **2009**, *42*, 925–937.
28. Moore, E. G.; Samuel, A. P. S.; Raymond, K. N. From Antenna to Assay: Lessons Learned in Lanthanide Luminescence. *Acc. Chem. Res.* **2009**, *42*, 542–552.
29. Allain, C.; Faulkner, S. Photophysical Approaches to Responsive Optical Probes. *Future Med. Chem.* **2010**, *2*, 339–350.
30. Comby, S.; Bünzli, J.-C. G. Lanthanide Near-Infrared Luminescence in Molecular Probes and Devices. In *Handbook on the Physics and Chemistry of Rare Earths*; Gschneidner, K. A. Jr., Bünzli, J.-C. G., Pecharsky, V. K., Eds.; Elsevier Science B.V.: Amsterdam, 2007; Vol. 37, pp 217–470.
31. Zhang, H.; Xu, Y.; Yang, W.; Li, Q. Dual-Lanthanide-Chelated Silica Nanoparticles as Labels for Highly Sensitive Time-Resolved Fluorometry. *Chem. Mater.* **2007**, *19*, 5875–5881.
32. Eliseeva, S. V.; Song, B.; Vandevyver, C. D. B.; Chauvin, A. S.; Wacker, J. B.; Bunzli, J. C. Increasing the Efficiency of Lanthanide Luminescent Bioprobes: Bioconjugated Silica Nanoparticles as Markers for Cancerous Cells. *New J. Chem.* **2010**, *34*, 2915–2921.
33. Samuel, J.; Tallec, G.; Cherns, P.; Ling, W. L.; Raccurt, O.; Poncelet, O.; Imbert, D.; Mazzanti, M. Lanthanide-Chelate Silica Nanospheres as Robust Multicolor Vis-NIR Tags. *Chem. Commun.* **2010**, *46*, 2647–2649.

34. Ai, K. L.; Zhang, B. H.; Lu, L. H. Europium-Based Fluorescence Nanoparticle Sensor for Rapid and Ultrasensitive Detection of an Anthrax Biomarker. *Angew. Chem., Int. Ed.* **2009**, *48*, 304–308.
35. Huhtinen, P.; Kivela, M.; Kuronen, O.; Hagren, V.; Takalo, H.; Tenhu, H.; Lovgren, T.; Harma, H. Synthesis, Characterization, and Application of Eu(III), Tb(III), Sm(III), and Dy(III) Lanthanide Chelate Nanoparticle Labels. *Anal. Chem.* **2005**, *77*, 2643–2648.
36. Vancaeyzeele, C.; Ornatsky, O.; Baranov, V.; Shen, L.; Abdelrahman, A.; Winnik, M. A. Lanthanide-Containing Polymer Nanoparticles for Biological Tagging Applications: Nonspecific Endocytosis and Cell Adhesion. *J. Am. Chem. Soc.* **2007**, *129*, 13653–13660.
37. Charbonniere, L. J.; Hildebrandt, N.; Ziessel, R. F.; Loehmannsroeben, H. G. Lanthanides to Quantum Dots Resonance Energy Transfer in Time-Resolved Fluoro-Immunoassays and Luminescence Microscopy. *J. Am. Chem. Soc.* **2006**, *128*, 12800–12809.
38. Ipe, B. I.; Yoosaf, K.; Thomas, K. G. Functionalized Gold Nanoparticles as Phosphorescent Nanomaterials and Sensors. *J. Am. Chem. Soc.* **2006**, *128*, 1907–1913.
39. Lewis, D. J.; Day, T. M.; MacPherson, J. V.; Pikramenou, Z. Luminescent Nanobeads: Attachment of Surface Reactive Eu(III) Complexes to Gold Nanoparticles. *Chem. Commun.* **2006**, 1433–1435.
40. Massue, J.; Quinn, S. J.; Gunnlaugsson, T. Lanthanide Luminescent Displacement Assays: The Sensing of Phosphate Anions Using Eu(III)-Cyclen-Conjugated Gold Nanoparticles in Aqueous Solution. *J. Am. Chem. Soc.* **2008**, *130*, 6900–6901.
41. Bonnet, C. S.; Massue, J.; Quinn, S. J.; Gunnlaugsson, T. Lanthanide Luminescent Gold Nanoparticles: pH-Driven Self-Assembly Formation Between Eu(III)-Cyclen Conjugated AuNPs and Sensitising Beta-Diketonate Antenna in Water. *Org. Biomol. Chem.* **2009**, *7*, 3074–3078.
42. Leonard, J. P.; dos Santos, C. M. G.; Plush, S. E.; McCabe, T.; Gunnlaugsson, T. pH Driven Self-Assembly of a Ternary Lanthanide Luminescence Complex: The Sensing of Anions Using a β-Diketonate-Eu(III) Displacement Assay. *Chem. Commun.* **2007**, 129–131.
43. Massue, J.; Plush, S. E.; Bonnet, C. S.; Moore, D. A.; Gunnlaugsson, T. Selective Mono N-Alkylations of Cyclen in One Step Syntheses. *Tetrahedron Lett.* **2007**, *48*, 8052–8055.
44. Murray, N. S.; Jarvis, S. P.; Gunnlaugsson, T. Luminescent Self-Assembly Formation on a Gold Surface Observed by Reversible 'Off-On' Switching of Eu(III) Emission. *Chem. Commun.* **2009**, 4959–4961.
45. Lynch, I.; Dawson, K. A. Protein-Nanoparticle Interactions. *Nano Today* **2008**, *3*, 40–47.
46. De Paoli Lacerda, S. H.; Park, J. J.; Meuse, C.; Pristinski, D.; Becker, M. L.; Karim, A.; Douglas, J. F. Interaction of Gold Nanoparticles with Common Human Blood Proteins. *ACS Nano* **2010**, *4*, 365–379.
47. Li, L.; Mu, Q.; Zhang, B.; Yan, B. Analytical Strategies for Detecting Nanoparticle-Protein Interactions. *Analyst (Cambridge, U. K.)* **2010**, *135*, 1519–1530.
48. Lin, J.; Zhang, H.; Chen, Z.; Zheng, Y. Penetration of Lipid Membranes by Gold Nanoparticles: Insights into Cellular Uptake, Cytotoxicity, and Their Relationship. *ACS Nano* **2010**, *4*, 5421–5429.
49. Walczyk, D.; Bombelli, F. B.; Monopoli, M. P.; Lynch, I.; Dawson, K. A. What the Cell Sees in Bionanoscience. *J. Am. Chem. Soc.* **2010**, *132*, 5761–5768.
50. Mahmood, M.; Casciano, D. A.; Mocan, T.; Iancu, C.; Xu, Y.; Mocan, L.; Iancu, D. T.; Dervishi, E.; Li, Z.; Abdalmuhsen, M.; *et al*. Cytotoxicity and Biological Effects of Functional Nanomaterials Delivered to Various Cell Lines. *J. Appl. Toxicol.* **2010**, *30*, 74–83.
51. Rivera Gil, P.; Oberdörster, G.; Elder, A.; Puntes, V.; Parak, W. J. Correlating Physico-Chemical with Toxicological Properties of Nanoparticles: The Present and the Future. *ACS Nano* **2010**, *4*, 5527–5531.
52. Caravan, P. Protein-Targeted Gadolinium-Based Magnetic Resonance Imaging (MRI) Contrast Agents: Design and Mechanism of Action. *Acc. Chem. Res.* **2009**, *42*, 851–862.
53. Thompson, M. K.; Doble, D. M. J.; Tso, L. S.; Barra, S.; Botta, M.; Aime, S.; Raymond, K. N. Hetero-Tripodal Hydroxypyridonate Gadolinium Complexes: Syntheses, Relaxometric Properties, Water Exchange Dynamics, and Human Serum Albumin Binding. *Inorg. Chem.* **2004**, *43*, 8577–8586.
54. Montgomery, C. P.; New, E. J.; Parker, D.; Peacock, R. D. Enantioselective Regulation of a Metal Complex in Reversible Binding to Serum Albumin: Dynamic Helicity Inversion Signalled by Circularly Polarised Luminescence. *Chem. Commun.* **2008**, 4261–4263.
55. Law, G. L.; Pal, R.; Palsson, L. O.; Parker, D.; Wong, K. L. Responsive and Reactive Terbium Complexes with an Azaxanthone Sensitiser and One Naphthyl Group: Applications in Ratiometric Oxygen Sensing *In Vitro* and in Regioselective Cell Killing. *Chem. Commun.* **2009**, 7321–7323.
56. Aime, S.; Gianolio, E.; Terreno, E.; Giovenzana, G. B.; Pagliarin, R.; Sisti, M.; Palmisano, G.; Botta, M.; Lowe, M. P.; Parker, D. Ternary Gd(III)L-HSA Adducts: Evidence for the Replacement of Inner-Sphere Water Molecules by Coordinating Groups of the Protein. Implications for the Design of Contrast Agents for MRI. *J. Biol. Inorg. Chem.* **2000**, *5*, 488–497.
57. Raghunand, N.; Guntle, G. P.; Gokhale, V.; Nichol, G. S.; Mash, E. A.; Jagadish, B. Design, Synthesis, and Evaluation of 1,4,7,10-Tetraazacyclododecane-1,4,7-triacetic Acid Derived, Redox-Sensitive Contrast Agents for Magnetic Resonance Imaging. *J. Med. Chem.* **2010**, *53*, 6747–6757.
58. Fung, Y. O.; Wu, W.; Yeung, C. T.; Kong, H. K.; Wong, K. K.-C.; Lo, W. S.; Law, G. L.; Wong, K. L.; Lau, C. K.; Lee, C. S.; *et al*. *In Vitro* Imaging and Human Serum Albumin Responsive Dimeric Lanthanide DO3A Complex. *Inorg. Chem.* **2011**, *50*, 5517–5525.
59. Peters, T. Jr. In *All about Albumin: Biochemistry, Genetics, and Medical Applications*; Academic Press: San Diego, CA, 1995.
60. Xie, H.; Tkachenko, A. G.; Glomm, W. R.; Ryan, J. A.; Brennaman, M. K.; Papanikolas, J. M.; Franzen, S.; Feldheim, D. L. Critical Flocculation Concentrations, Binding Isotherms, and Ligand Exchange Properties of Peptide-Modified Gold Nanoparticles Studied by UV-Visible, Fluorescence, and Time-Correlated Single Photon Counting Spectroscopies. *Anal. Chem.* **2003**, *75*, 5797–5805.
61. Binnemans, K. Rare Earth β-Diketonate Complexes: Functionalities and Applications. In *Handbook on the Physics and Chemistry of Rare Earths*; Gschneidner, K. A. Jr., Bünzli, J.-C. G., Pecharsky, V. K., Eds.; Elsevier Science B.V.: Amsterdam, 2005; Vol. 35, pp 107–272.
62. Bourassa, P.; Kanakis, C. D.; Tarantilis, P.; Pollissiou, M. G.; Tajmir-Riahi, H. A. Resveratrol, Genistein, and Curcumin Bind Bovine Serum Albumin. *J. Phys. Chem. B* **2010**, *114*, 3348–3354.
63. Lakowicz, J. R. In *Principles of Fluorescence Spectroscopy*, 3rd ed.; Springer Science: New York, 2006.
64. Tian, F. F.; Jiang, F. L.; Han, X. L.; Xiang, C.; Ge, Y. S.; Li, J. H.; Zhang, Y.; Li, R.; Ding, X. L.; Liu, Y. Synthesis of a Novel Hydrazone Derivative and Biophysical Studies of Its Interactions with Bovine Serum Albumin by Spectroscopic, Electrochemical, and Molecular Docking Methods. *J. Phys. Chem. B* **2010**, *114*, 14842–14853.
65. Kragh-Hansen, U. Molecular Aspects of Ligand Binding to Serum Albumin. *Pharmacol. Rev.* **1981**, *33*, 17–53.
66. Kratochwil, N. A.; Huber, W.; Müller, F.; Kansy, M.; Gerber, P. R. Predicting Plasma Protein Binding of Drugs: A New Approach. *Biochem. Pharmacol.* **2002**, *64*, 1355–1374.
67. Gampp, H.; Maeder, M.; Meyer, C. J.; Zuberbühler, A. D. Calculation of Equilibrium Constants from Multiwavelength Spectroscopic Data - I. Mathematical Consideration. *Talanta* **1985**, *32*, 95–101.
68. Gampp, H.; Maeder, M.; Meyer, C. J.; Zuberbühler, A. D. Calculation of Equilibrium Constants from Multiwavelength Spectroscopic Data - IV. Model-Free Least-Squares Refinement by Use of Evolving Factor Analysis. *Talanta* **1986**, *33*, 943–951.

69. Togashi, D. M.; Ryder, A. G.; Mc, M.; Dunne, P.; McManus, J. Fluorescence Study of Bovine Serum Albumin and Ti and Sn Oxide Nanoparticles Interactions. *Proc. SPIE* **2007**, *6628*, 66281K1–11.
70. Goutelle, S.; Maurin, M.; Rougier, F.; Barbaut, X.; Bourguignon, L.; Ducher, M.; Maire, P. The Hill Equation: a Review of Its Capabilities in Pharmacological Modelling. *Fundam. Clin. Pharmacol.* **2008**, *22*, 633–648.
71. Kitamura, K.; Kume, M.; Yamamoto, M.; Takegami, S.; Kitade, T. ^{19}F NMR Spectroscopic Study on the Binding of Triflupromazine to Bovine and Human Serum Albumins. *J. Pharm. Biomed. Anal.* **2004**, *36*, 411–414.
72. Varlan, A.; Hillebrand, M. Bovine and Human Serum Albumin Interactions with 3-Carboxyphenoxathiin Studied by Fluorescence and Circular Dichroism Spectroscopy. *Molecules* **2010**, *15*, 3905–3919.
73. Tian, J.; Zhao, Y.; Liu, X.; Zhao, S. A Steady-State and Time-Resolved Fluorescence, Circular Dichroism Study on the Binding of Myricetin to Bovine Serum Albumin. *Luminescence* **2009**, *24*, 386–393.
74. Johnson, W. C. Protein Secondary Structure and Circular Dichroism: A Practical Guide. *Proteins* **1990**, *7*, 205–214.
75. Bardhan, M.; Mandal, G.; Ganguly, T. Steady State, Time Resolved, and Circular Dichroism Spectroscopic Studies to Reveal the Nature of Interactions of Zinc Oxide Nanoparticles with Transport Protein Bovine Serum Albumin and to Monitor the Possible Protein Conformational Changes. *J. Appl. Phys.* **2009**, *106*, 034701–034705.
76. He, X. M.; Carter, D. C. Atomic Structure and Chemistry of Human Serum Albumin. *Nature* **1992**, *358*, 209–215.
77. Ni, Y.; Zhang, Q.; Kokot, S. Analysis of the Interactions of Mixtures of Two [Small Beta]-Agonists Steroids with Bovine Serum Albumin: a Fluorescence Spectroscopy and Chemometrics Investigation. *Analyst (Cambridge, U. K.)* **2010**, *135*, 2059–2068.
78. Böhm, G.; Muhr, R.; Jaenicke, R. Quantitative Analysis of Protein Far UV Circular Dichroism Spectra by Neural Networks. *Protein Eng.* **1992**, *5*, 191–195.
79. Kamiya, M.; Johnsson, K. Localizable and Highly Sensitive Calcium Indicator Based on a BODIPY Fluorophore. *Anal. Chem.* **2010**, *82*, 6472–6479.
80. Motulsky, H.; Christopoulos, A. In *Fitting Models to Biological Data Using Linear and Nonlinear Regression*; Oxford University Press: New York, USA, 2004.